Accurate characterization of tip-induced potential using electron interferometry

A. Iordanescu, S. Toussaint, G. Bachelier, S. Fallahi, C. Gardner, M. Manfra, B. Hackens, B. Brun

Applied Physics Letters ARTICLE scitation.org/journal/apl

Accurate characterization of tip-induced potential using electron interferometry

Cite as: Appl. Phys. Lett. **117**, 193101 (2020); doi: 10.1063/5.0023698
Submitted: 31 July 2020 · Accepted: 18 October 2020 ·
Published Online: 9 November 2020

A. Iordanescu,[1] S. Toussaint,[1] G. Bachelier,[2] S. Fallahi,[3,4] C. G. Gardner,[4,5] M. J. Manfra,[3,4,5,6,7] B. Hackens,[1] and B. Brun[1,a)]

AFFILIATIONS

[1]IMCN/NAPS, Université Catholique de Louvain (UCLouvain), 1348 Louvain-la-Neuve, Belgium
[2]CNRS, Institut Néel, F-38042 Grenoble, France
[3]Department of Physics and Astronomy, Purdue University, West Lafayette, Indiana 47907, USA
[4]Birck Nanotechnology Center, Purdue University, West Lafayette, Indiana 47907, USA
[5]Microsoft Quantum Purdue, Purdue University, West Lafayette, Indiana 47907, USA
[6]School of Electrical and Computer Engineering, Purdue University, West Lafayette, Indiana 47907, USA
[7]School of Materials Engineering, Purdue University, West Lafayette, Indiana 47907, USA

[a)]**Author to whom correspondence should be addressed:** boris.brun@wanadoo.fr

ABSTRACT

Using the tip of a scanning probe microscope as a local electrostatic gate gives access to real-space information on electrostatics as well as charge transport at the nanoscale, provided that the tip-induced electrostatic potential is well known. Here, we focus on the accurate characterization of the tip potential, in a regime where the tip locally depletes a two-dimensional electron gas (2DEG) hosted in a semiconductor heterostructure. Scanning the tip in the vicinity of a quantum point contact defined in the 2DEG, we observe Fabry–Pérot interference fringes at low temperature in maps of the device conductance. We exploit the evolution of these fringes with the tip voltage to measure the change in the depletion radius by electron interferometry. We find that a semi-classical finite-element self-consistent model taking into account the conical shape of the tip reaches a faithful correspondence with the experimental data.

Scanning Gate Microscopy (SGM) was invented more than 20 years ago,[1] with the objective to probe electron transport at the local scale inside confined electronic systems. SGM consists in locally altering the potential landscape experienced by charge carriers within an electronic device using the biased metallic tip of an Atomic Force Microscope (AFM), while recording the induced changes in the device conductance.[2] SGM was first developed to study electronic transport in high mobility two-dimensional electron gases (2DEGs) buried in III–V heterostructures. In these systems, direct probing of the local electronic density using scanning tunneling microscopy is prevented by the insulating layer separating the 2DEG from the surface. The first impressive breakthroughs provided by the SGM technique were the observation of branched electron flow within the 2DEGs,[3] as well as the ability to image electron wave-functions.[4] Since then, many groups developed SGM setups, and it proved to be a very useful tool to investigate mesoscopic transport at the local scale in various systems, such as quantum dots,[5–7] quantum rings,[8,9] magnetic focusing geometries,[10,11] and quantum Hall systems,[12–16] and even to explore subtle electron-electron interaction effects.[17–21] In the past decade, SGM has also been used to provide real-space data on transport through graphene mesoscopic devices.[22–27]

In all the above-mentioned cases, SGM relies on measuring the evolution of a device transport property under the influence of an external perturbation, i.e., the tip-induced electrostatic potential. The accurate knowledge of this perturbation potential is, therefore, a crucial issue in the interpretation of the SGM signal. Usually, this potential is estimated in the experiment using its direct effect on transport through a Quantum Point Contact (QPC)[28] or a quantum dot,[29–31] when the polarized tip scans in the vicinity of the device. However, the latter method suffers from the screening from the top metallic gates, which has been shown to significantly distort the tip-induced potential.[32]

In the present work, we devise an original way to precisely evaluate the size of the tip-induced depletion region in a high-mobility 2DEG, relying on electron interferometry. We apply a negative voltage to the metallic tip of an AFM to locally deplete the 2DEG and form a

Fabry–Pérot (FP) cavity between a QPC and the depleted area below the tip. Following the evolution of a single interference fringe with the tip voltage, we can precisely measure the radius of the depleted region. This approach is advantageous compared to previous techniques, as the tip-induced perturbation is measured in a pristine area of the 2DEG, without suffering from metallic gate screening. We justify the assumptions underlying the experimental method using tight-binding simulations. Finally, we propose different electrostatic models to reproduce the tip-induced depletion region, in a semi-classical approximation. We demonstrate that the potential induced by a charged sphere and screened by the 2DEG correctly predicts the depletion threshold, but fails to describe the depleted area radius. Finally, we show that modeling the tip as a cone and calculating self-consistently the electrostatic potential reproduce very well the experimental trend.

We study a QPC[33,34] defined using metallic gates deposited on top of an $Al_{0.3}Ga_{0.7}As/GaAs$ heterostructure hosting a 2DEG with a density of $n_s = 2.53 \times 10^{15}\,m^{-2}$ and a mobility of $\mu = 3.25 \times 10^6\,cm^2/(V\,s)$, located $d = 57$ nm beneath the surface [see Fig. 1(a)]. The two metallic top gates are separated from each other by a gap of 300 nm. The sample is thermally anchored on the cold finger of a dilution refrigerator with a base temperature below 100 mK. The QPC conductance G is measured using a four contact lock-in technique at low frequency (77 Hz). This method consists in polarizing the device with an AC voltage V_{AC}, typically 10 μV, and simultaneously measuring the current I flowing through the device and the voltage drop V across the device. $G = I/V$ is plotted in Fig. 1(b) as a function of the voltage V_G applied on the top metallic gates. As V_G decreases toward negative values, G exhibits plateaus at integer multiples of $2e^2/h$, corresponding to the number of transverse quantum modes transmitted through the 1D channel between the gates. All subsequent scanning gate measurements were obtained with one quantum mode transmitted through the QPC.

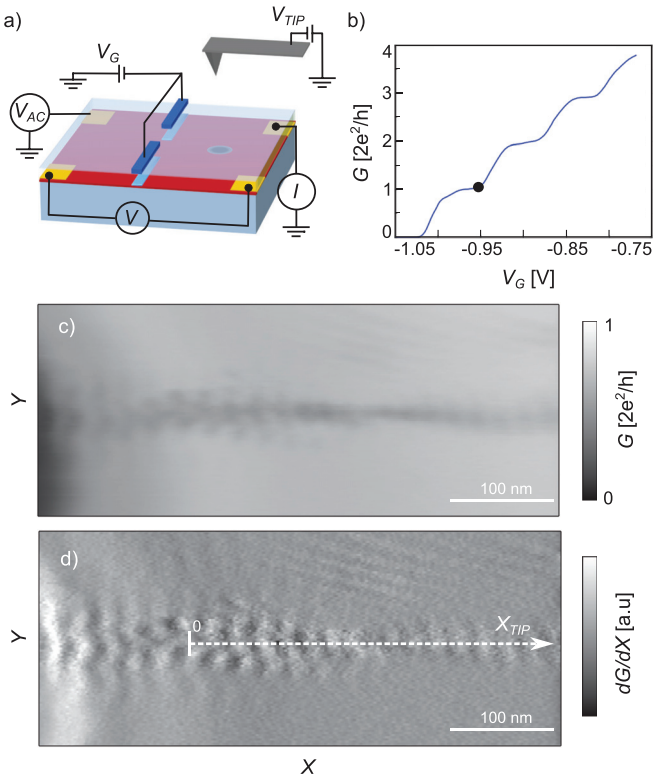

FIG. 1. (a) Schematic illustration of the scanning gate setup: top metallic gates defining the QPC are represented in blue, the 2DEG plane in red, and contacts in yellow. (b) Low temperature electrical conductance of the QPC vs V_G in units of $2e^2/h$. The black dot indicates the QPC polarization used for the SGM mappings. (c) SGM map of the QPC conductance acquired for $V_{TIP} = -6$ V and $d_{TIP} = 30$ nm, with a voltage of $V_G = -0.95$ V applied on the top metallic gates. (d) Numerical derivative of the data in (c), with respect to X. The horizontal axes are matched. The white dashed line corresponds to the X_{TIP} axis in the next figures, with $X_{TIP} = 0$ corresponding to the extremity of the left arrow.

To perform SGM measurements, a metallic tip (a Pt-coated AFM tip provided by μ-masch, model HQ:CSC17/PT[35]) acting as a local and movable gate, is brought in close proximity to the device surface, at a tip-surface vertical distance of $d_{TIP} = 30$ nm. Applying a negative voltage V_{TIP} on the tip induces a local perturbation for conduction electrons, which, in turn, alters the device conductance. G is recorded as a function of X and Y relative tip coordinates, yielding a SGM map. When a sufficiently large negative voltage is applied on the tip, the SGM map reveals a single rather straight branch of reduced conductance aligned with the QPC transport axis, decorated with transverse periodic oscillations. This is illustrated in Fig. 1(c), showing the SGM map acquired for $V_{TIP} = -6$ V in a rectangular region located next to the QPC (the QPC is located 500 nm beyond the left edge of the figure).

The commonly accepted interpretation for the origin of periodic oscillation is based on the formation of a Fabry–Pérot-like interferometer for electrons.[3,36] In this picture, the two mirrors forming the Fabry–Pérot (FP) cavity are the QPC on one side and the tip-induced depleted region on the other side. Shifting the tip position successively switches the interference condition between constructive and destructive, leading to an oscillating contrast in the conductance map. The oscillation period should then be given by half of the Fermi wavelength, λ_F. From Fig. 1(d), one can extract $\lambda_F/2 \simeq 20$ nm, close to the expected value, given the electronic density ($\lambda_F/2 = \sqrt{2\pi/n_s}/2 = 24$ nm), which is consistent with the FP interpretation.

In the remainder of this paper, we will exploit the interference pattern to extract quantitative information on the shape of the tip-induced perturbation. The key data are plotted in Fig. 2(a), showing the evolution of the interference patterns as a function of the tip voltage while scanning along the white dashed line in Fig. 1(d), corresponding to the X_{TIP} axis. The first quantity that can be extracted from these data is the radius of the tip-induced depletion region R_{TIP}. In principle, to keep the size of the FP cavity constant when V_{TIP} evolves toward more negative values, the tip has to be moved away from the QPC [as illustrated in Fig. 2(b)]. Hence, each iso-conductance line in the interference pattern actually corresponds to an iso-sized FP cavity: as one follows an interference line, a variation of the tip voltage ΔV_{TIP} beyond the onset of 2DEG depletion translates directly into a variation of R_{TIP}, measured as ΔX_{TIP}, and the shift in the tip position to keep a constant cavity size ($R_{TIP} = 0$ nm corresponds to the onset of the interference, see below). For example, when changing V_{TIP} from -4.5 V [onset of depletion, yellow dot in Fig. 2(a)] to -8 V ($\Delta V_{TIP} = -3.5$ V), the required change in the tip position to remain on the same interference fringe is $\Delta X_{TIP} \sim 120$ nm from the data in

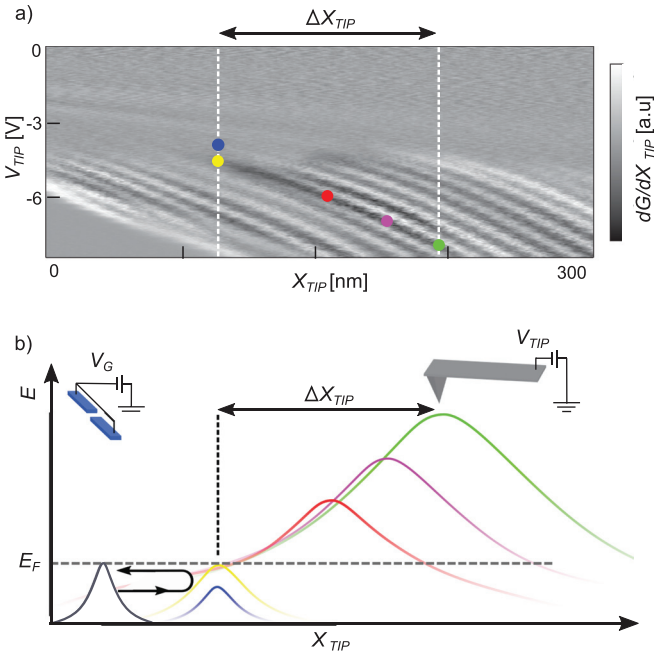

FIG. 2. (a) Derivative of G with respect to X_{TIP} along the white dashed line in Fig. 1(d), plotted as a function of V_{TIP} for a tip-sample distance of $d_{TIP} = 30$ nm and a gate voltage of $V_G = -0.92$ V. Except for the blue dot (corresponding to $V_{TIP} = -4$ V), the other colored dots correspond to (X_{TIP}, V_{TIP}) coordinates following the same interference line: yellow dot for $V_{TIP} = -4.5$ V, red dot for $V_{TIP} = -6$ V, pink dot for $V_{TIP} = -7$ V, and green dot for $V_{TIP} = -8$ V. (b) Schematics of the energy landscape induced by the top gates (dark curve) and by the tip (colored curves) for the same (X_{TIP}, V_{TIP}) coordinates indicated in (a). For $V_{TIP} = -4$ V, the tip-induced perturbation is not strong enough to reach the Fermi energy $E_F = 4.5$ meV and electrons are not backscattered.

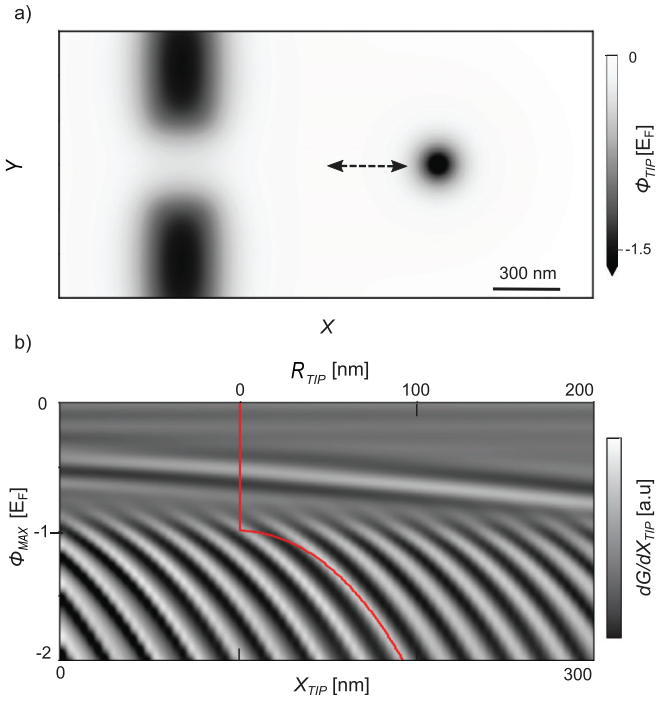

FIG. 3. (a) Illustration of the electrostatic potential below the finger gates and the tip (dark areas are depleted). (b) Line profiles of the derivative of the simulated G along the black dashed line in (a) (i.e., the X_{TIP} axis), as a function of the maximum of the tip-induced perturbation, normalized in units of Fermi energy. The red curve corresponds to the radius of the depletion region (R_{TIP} top axis) calculated using Eq. (1).

Fig. 2(a) (consider, e.g., the yellow and green dots), leading to a tip-induced depletion region with a radius of $R_{TIP} \sim 120$ nm.

This experimental method to determine R_{TIP} relies on two main assumptions: (i) interference fringes are observed as soon as the maximum of the tip-induced perturbation reaches the Fermi energy (i.e., the depletion threshold) and (ii) the turning point of the electrons in the tip-induced depletion region follows the exact depletion limit. To justify both non-trivial assumptions, we perform tight-binding simulations using the Kwant python package.[37] We scale all the energies and distances to match the experimental conditions. We model the QPC gate potential using the method proposed by Davies *et al.*,[38] and let only one single mode be transmitted through the QPC. We model the tip using an approximate solution for the potential $\phi_{TIP}(r)$ induced at a distance r by a screened charged sphere of radius R_S, in the Thomas–Fermi approximation:[39]

$$\phi_{TIP}(r) = \frac{R_S V_{tip}}{\epsilon_r} \int_0^\infty q\, J_0(qr) \frac{e^{-qd}}{q + q_{TF}}\, dq, \qquad (1)$$

where J_0 is the zeroth-order Bessel function and q_{TF} the Thomas–Fermi wave-vector, which we assume to be $2/a_0$, with $a_0 = \frac{4\pi\epsilon\epsilon_0\hbar^2}{m^* e^2} \simeq 10$ nm being the effective Bohr radius for electrons in GaAs.[31,38,40,41] The electrostatic potential landscape in our simulation is shown in Fig. 3(a).

We calculate the total system transmission as a function of the position of this perturbation potential at a variable distance X_{TIP} from the QPC, with $X_{TIP} = 0$ nm corresponding to 500 nm away from the QPC [the X_{TIP} axis corresponds to the black dashed line in Fig. 3(a)]. We differentiate the calculated transmission vs X_{TIP} and plot the result in Fig. 3(b), as a function of X_{TIP} and the maximum potential induced by the tip in the 2DEG plane ϕ_{MAX}, normalized to E_F. The result appears very similar to the experiment [Fig. 2(a)], and the interference fringes start to be contrasted below a voltage threshold ϕ_{MAX} very close to the Fermi energy. For $|\phi_{MAX}| > E_F$, the fringe contrast is constant.

This provides a validation for hypothesis (i): the threshold for the emergence of FP interferences indeed corresponds to the 2DEG depletion. We also plot in Fig. 3(b) the depletion radius R_{TIP} found from Eq. (1) (red curve). Below the depletion threshold and when the depletion spot is well defined and large enough, the FP interference fringes evolve in a way that exactly matches the evolution of the depletion zone, indicating that the turning point is indeed the limit of the depleted area. This simulation, therefore, also justifies assumption (ii). A discrepancy can, however, be noted when the tip-induced potential is very close to the Fermi energy, where assumption (ii) does not hold anymore, since the turning point is not given by the depleted limit, either when the tip-induced potential does not deplete the 2DEG but generates efficient backscattering ($\phi_{MAX} \gtrsim E_F$) or when the tip just slightly depletes the 2DEG and the wave-function leaks into the

shallow-depleted region ($\phi_{MAX} \lesssim E_F$). This slight discrepancy induces a few percent of uncertainty in the evaluation of the total depletion spot radius but leaves unchanged the conclusions regarding the ability to precisely follow the depletion spot evolution with tip voltage at sufficiently negative V_{TIP}.

Next, we compare the outcome of simple electrostatic models of the tip perturbation, taking into account the screening of the 2DEG, with the experimental data. We first consider the analytical tip-2DEG model described by Eq. (1). In this first model [1, in Fig. 4(a)], the conductive sphere is positioned at a vertical distance $d_{TIP-2DEG}$ from the 2DEG and we neglect the top dielectric layers of $Al_{0.3}Ga_{0.7}As$ and GaAs. Figure 4(b) (black continuous curve) shows the electrostatic potential profile calculated in the 2DEG, for a distance of $d_{TIP-2DEG} = 87$ nm, a radius of $R_S = 50$ nm, while taking $\epsilon_r = 10.62$ and $q_{TF} = 0.2\,\mathrm{nm}^{-1}$ for the substrate GaAs layer. When compared with the experimental data in Fig. 4(c), the shape of the tip-induced potential obtained using Eq. (1) [continuous black curve in Fig. 4(c)] does not correspond to the iso-conductance lines in the FP interference pattern. This can be explained in light of the approximations used in this model: the dielectric layers above the 2DEG are neglected, as well as the full shape of the tip (assuming that it has a spherical shape). Moreover, changes in the screening of the tip potential due to the emergence of a tip-induced depleted region are not taken into account. In the real device, the 2DEG is housed between a top $Al_{0.3}Ga_{0.7}As$ layer with a thickness d and a GaAs substrate, the experimental AFM tip has a cone-like shape as illustrated in the inset of Fig. 4(b), and screening phenomena are more complex than the simple description given by Eq. (1).

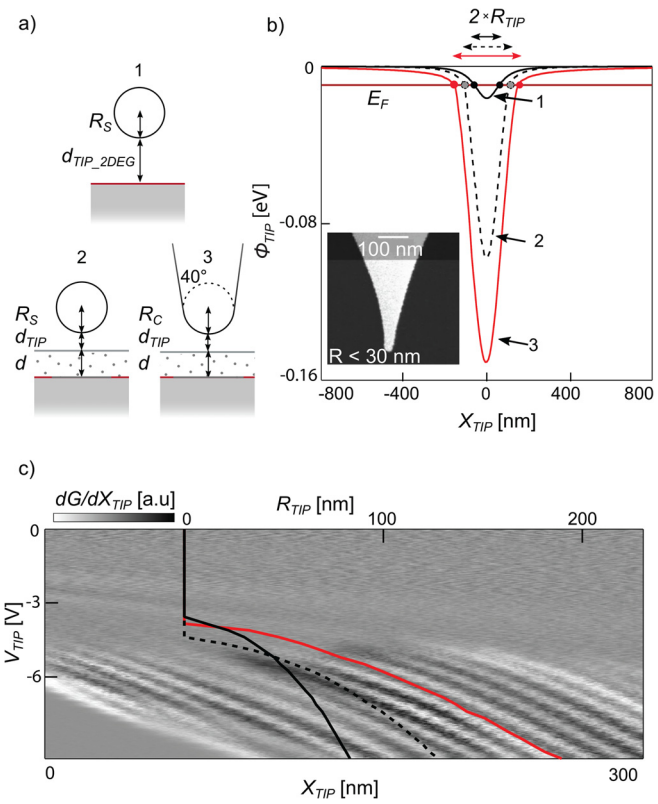

FIG. 4. (a) Illustration of the three tip-2DEG models: the red line corresponds to the 2DEG layer, the gray layer corresponds to the GaAs layer, while the dotted layer corresponds to the AlGaAs layer. (b) Tip potential profiles traced for the three models presented in (a), for $V_{TIP} = -7$ V: (1) a spherical tip in an analytical non-self-consistent framework (continuous black line), (2) a spherical tip in a finite element self-consistent model (dotted black line), and (3) a conical tip in a finite element self-consistent model (red line). The inset shows a side-view electron micrograph of a PtIr tip similar to the one used in the experiment[35] (reproduced with permission from MikroMasch). The horizontal line corresponds to $E_F = -9.6$ meV. The crossing between the Fermi energy and the tip potential profile determines the diameter tip-induced depletion area. (c) Evolution of line profiles of the derivative of conductance with respect to X_{TIP}, recorded as a function of V_{TIP}, while the tip scans at $d_{TIP} = 30$ nm. The curves represent the tip-induced depletion radius (R_{TIP}, top axis) extracted for the three models presented in (a).

To determine the shape of the tip-induced perturbation in a scenario closer to the experimental situation, we simulated the associated electrostatic problem using the Comsol® software. It consists in finite element simulation of the electromagnetic field in a region of space where the metallic parts, the dielectric, the doping layer, and the 2DEG are defined. Then, the Poisson equation is solved by successive iterations, which, in turn, provides the local potential as well as the local electronic density in the depleted 2DEG. In this scenario, the 2DEG lies at $d = 57$ nm beneath the surface, between the $Al_{0.3}Ga_{0.7}As$ layer and the GaAs substrate. We assume a relative permittivity of $\epsilon_r = 10.17$ for the $Al_{0.3}Ga_{0.7}As$ layer. We neglect the GaAs substrate permittivity ($\epsilon_r = 10.62$), as the layer is considered infinitely thin in the simulations. The doping layer is modeled as a uniformly charged plane, with a density of $2.53 \times 10^{15}\,\mathrm{m}^{-2}$, insensitive to the local potential and coinciding with the 2DEG plane. When no voltage is applied neither on gates nor on the tip, the electron density is $2.53 \times 10^{15}\,\mathrm{m}^{-2}$.

We consider two models for the tip, as represented in Fig. 4(a): a sphere with a radius R_S (model 2) and a cone with a spherical apex with a curvature radius of $R_C = 50$ nm and a full tip cone angle of 40° (model 3), both placed at $d_{TIP} = 30$ nm from the surface of the sample. For each model, we extract the radius of the tip-induced depletion from the simulated electrostatic potential profile in the 2DEG plane [shown in Fig. 4(b)] and compare it to the outcome of the classical electrostatic model discussed above and to the experimental data [Fig. 4(c)]. Compared to model (1), we observe that R_{TIP} vs V_{TIP} estimated using model (2) is closer to the experimental data [Fig. 4(c), dashed line]: it indeed yields a faster evolution of R_{TIP} with V_{TIP}, due to the absence of screening of the tip potential by the depleted region below the tip. However, model (2) still underestimates the depletion spot size compared to the experimental data: the variation of R_{TIP} with V_{TIP} [the dashed line in Fig. 4(c)] is slower than the evolution of FP interferences. Model (3) [red curve in Figs. 4(b) and 4(c)] yields the most faithful estimate of R_{TIP} with V_{TIP} compared to the experimental result, e.g., for a change in the tip voltage of $\Delta V_{TIP} = 3.5$ V in the range considered in the experiment (from -4.5 V to -8 V), and the increase in $R_{TIP} \sim 120$ nm, i.e., the same value estimated above from the experiment. Furthermore, the non-linear shape of the calculated tip-induced depletion fully reproduces isophase interference profiles observed in the experiment. The last model can, therefore, serve as reference to evaluate the tip-induced depletion region shape and size.

In conclusion, we performed electron interferometry using a scanning gate microscope, in order to precisely evaluate the size of the

depletion radius induced by a polarized SGM tip. We showed that the evolution of interference fringes allows us to accurately estimate the depletion radius dependence on tip voltage and justified this approach using tight-binding simulations of quantum transport. A simple electrostatic model of the potential created by a charged sphere and screened by a 2DEG is sufficient to predict the depletion threshold, but underestimates the size of the depletion spot. Finally, we showed that a complete modeling of the tip geometry including its conic tail accurately describes the tip-induced depletion region. This provides new guidelines to choose the best approach to model SGM experiments, in particular, when the tip is used as a tunable and movable depleting scatterer.[42,43]

See the supplementary material for further details regarding tight-binding simulations and the analytical model for the screened tip-induced potential.

The present research was partly funded by the Fédération Wallonie-Bruxelles through ARC Grant No. 16/21-077 and by the F.R.S-FNRS through Grant No. J008019F. B.B. (research assistant), B.H. (research associate), and A.I. (FRIA fellowship) acknowledge financial support from the F.R.S.-FNRS of Belgium.

DATA AVAILABILITY

The data that support the findings of this study are available from the corresponding author upon reasonable request.

REFERENCES

[1]M. A. Eriksson, R. G. Beck, M. Topinka, J. A. Katine, R. M. Westervelt, K. L. Campman, and A. C. Gossard, Appl. Phys. Lett. **69**, 671 (1996).
[2]H. Sellier, B. Hackens, M. Pala, F. Martins, S. Baltazar, X. Wallart, L. Desplanque, V. Bayot, and S. Huant, Semicond. Sci. Technol. **26**, 064008 (2011).
[3]M. Topinka, B. J. LeRoy, R. Westervelt, S. Shaw, R. Fleischmann, E. Heller, K. Maranowski, and A. Gossard, Nature **410**, 183 (2001).
[4]M. Topinka, B. J. LeRoy, S. Shaw, E. Heller, R. Westervelt, K. Maranowski, and A. Gossard, Science **289**, 2323 (2000).
[5]P. Fallahi, A. C. Bleszynski, R. M. Westervelt, J. Huang, J. D. Walls, E. J. Heller, M. Hanson, and A. C. Gossard, Nano Lett. **5**, 223 (2005).
[6]A. C. Bleszynski, F. A. Zwanenburg, R. Westervelt, A. L. Roest, E. P. Bakkers, and L. P. Kouwenhoven, Nano Lett. **7**, 2559 (2007).
[7]M. Huefner, C. May, S. Kičin, K. Ensslin, T. Ihn, M. Hilke, K. Suter, N. de Rooij, and U. Staufer, Phys. Rev. B **79**, 134530 (2009).
[8]B. Hackens, F. Martins, T. Ouisse, H. Sellier, S. Bollaert, X. Wallart, A. Cappy, J. Chevrier, V. Bayot, and S. Huant, Nat. Phys. **2**, 826 (2006).
[9]F. Martins, B. Hackens, M. Pala, T. Ouisse, H. Sellier, X. Wallart, S. Bollaert, A. Cappy, J. Chevrier, V. Bayot *et al.*, Phys. Rev. Lett. **99**, 136807 (2007).
[10]K. E. Aidala, R. E. Parrott, T. Kramer, E. Heller, R. Westervelt, M. P. Hanson, and A. C. Gossard, Nat. Phys. **3**, 464 (2007).
[11]S. Bhandari, G.-H. Lee, A. Klales, K. Watanabe, T. Taniguchi, E. Heller, P. Kim, and R. M. Westervelt, Nano Lett. **16**, 1690 (2016).
[12]B. Hackens, F. Martins, S. Faniel, C. A. Dutu, H. Sellier, S. Huant, M. Pala, L. Desplanque, X. Wallart, and V. Bayot, Nat. Commun. **1**, 39 (2010).
[13]N. Paradiso, S. Heun, S. Roddaro, L. Sorba, F. Beltram, G. Biasiol, L. Pfeiffer, and K. West, Phys. Rev. Lett. **108**, 246801 (2012).
[14]M. Connolly, R. Puddy, D. Logoteta, P. Marconcini, M. Roy, J. Griffiths, G. Jones, P. Maksym, M. Macucci, and C. Smith, Nano Lett. **12**, 5448 (2012).
[15]F. Martins, S. Faniel, B. Rosenow, M. Pala, H. Sellier, S. Huant, L. Desplanque, X. Wallart, V. Bayot, and B. Hackens, New J. Phys. **15**, 013049 (2013).
[16]F. Martins, S. Faniel, B. Rosenow, H. Sellier, S. Huant, M. Pala, L. Desplanque, X. Wallart, V. Bayot, and B. Hackens, Sci. Rep. **3**, 1416 (2013).
[17]R. Crook, J. Prance, K. Thomas, S. Chorley, I. Farrer, D. Ritchie, M. Pepper, and C. Smith, Science **312**, 1359 (2006).
[18]M. Jura, M. Grobis, M. Topinka, L. Pfeiffer, K. West, and D. Goldhaber-Gordon, Phys. Rev. B **82**, 155328 (2010).
[19]B. Brun, F. Martins, S. Faniel, B. Hackens, G. Bachelier, A. Cavanna, C. Ulysse, A. Ouerghi, U. Gennser, D. Mailly *et al.*, Nat. Commun. **5**, 4290 (2014).
[20]B. Brun, F. Martins, S. Faniel, B. Hackens, A. Cavanna, C. Ulysse, A. Ouerghi, U. Gennser, D. Mailly, P. Simon *et al.*, Phys. Rev. Lett. **116**, 136801 (2016).
[21]A. Iagallo, N. Paradiso, S. Roddaro, C. Reichl, W. Wegscheider, G. Biasiol, L. Sorba, F. Beltram, and S. Heun, Nano Res. **8**, 948 (2015).
[22]S. Schnez, J. Güttinger, M. Huefner, C. Stampfer, K. Ensslin, and T. Ihn, Phys. Rev. B **82**, 165445 (2010).
[23]N. Pascher, D. Bischoff, T. Ihn, and K. Ensslin, Appl. Phys. Lett. **101**, 063101 (2012).
[24]A. G. Garcia, M. König, D. Goldhaber-Gordon, and K. Todd, Phys. Rev. B **87**, 085446 (2013).
[25]D. Cabosart, A. Felten, N. Reckinger, A. Iordanescu, S. Toussaint, S. Faniel, and B. Hackens, Nano Lett. **17**, 1344 (2017).
[26]Z. Dou, S. Morikawa, A. Cresti, S.-W. Wang, C. G. Smith, C. Melios, O. Kazakova, K. Watanabe, T. Taniguchi, S. Masubuchi *et al.*, Nano Lett. **18**, 2530 (2018).
[27]B. Brun, N. Moreau, S. Somanchi, V.-H. Nguyen, K. Watanabe, T. Taniguchi, J.-C. Charlier, C. Stampfer, and B. Hackens, Phys. Rev. B **100**, 041401 (2019).
[28]R. Steinacher, A. A. Kozikov, C. Rössler, C. Reichl, W. Wegscheider, T. Ihn, and K. Ensslin, New J. Phys. **17**, 043043 (2015).
[29]A. Pioda, S. Kičin, T. Ihn, M. Sigrist, A. Fuhrer, K. Ensslin, A. Weichselbaum, S. E. Ulloa, M. Reinwald, and W. Wegscheider, Phys. Rev. Lett. **93**, 216801 (2004).
[30]A. Gildemeister, T. Ihn, M. Sigrist, K. Ensslin, D. Driscoll, and A. Gossard, Phys. Rev. B **75**, 195338 (2007).
[31]P. Liu, F. Martins, B. Hackens, L. Desplanque, X. Wallart, M. Pala, S. Huant, V. Bayot, and H. Sellier, Phys. Rev. B **91**, 075313 (2015).
[32]S. Schnez, J. Güttinger, C. Stampfer, K. Ensslin, and T. Ihn, New J. Phys. **13**, 053013 (2011).
[33]B. J. van Wees, H. van Houten, C. W. J. Beenakker, J. G. Williamson, L. P. Kouwenhoven, D. van der Marel, and C. T. Foxon, Phys. Rev. Lett. **60**, 848 (1988).
[34]D. A. Wharam, T. J. Thornton, R. Newbury, M. Pepper, H. Ahmed, J. E. F. Frost, D. G. Hasko, D. C. Peacock, D. A. Ritchie, and G. A. C. Jones, J. Phys. C **21**, L209 (1988).
[35]μMasch, see https://www.spmtips.com/conductive-afm-probes-30-nm-radius-tip-Pt-coated.html "AFM Conductive Tips" (last accessed December 2, 2019).
[36]B. J. LeRoy, A. Bleszynski, K. Aidala, R. Westervelt, A. Kalben, E. Heller, S. Shaw, K. Maranowski, and A. Gossard, Phys. Rev. Lett. **94**, 126801 (2005).
[37]C. W. Groth, M. Wimmer, A. R. Akhmerov, and X. Waintal, New J. Phys. **16**, 063065 (2014).
[38]J. H. Davies, *The Physics of Low-Dimensional Semiconductors: An Introduction* (Cambridge University Press, 1998).
[39]T. Ihn, *Semiconductor Nanostructures* (Oxford University Press, 2010).
[40]M. R. Krcmar and W. M. Saslow, Phys. Rev. B **66**, 235310 (2002).
[41]F. Stern, Phys. Rev. Lett. **18**, 546 (1967).
[42]A. A. Kozikov, D. Weinmann, C. Rössler, T. Ihn, K. Ensslin, C. Reichl, and W. Wegscheider, Phys. Rev. B **94**, 195428 (2016).
[43]S. Toussaint, B. Brun, S. Faniel, L. Desplanque, X. Wallart, V. Bayot, and B. Hackens, Phys. Rev. B **98**, 075310 (2018).